Lin *et al. Chem Synth* 2024;4:32
DOI: 10.20517/cs.2024.17

Chemical Synthesis

Research Article

Open Access

Facile synthesis of Ag/AgCl/PAF-54 heterojunction photocatalysts for TC degradation

Yonghui Lin, Letian Gan, Xiaojun Zhao*, Guang Che, Shicheng Wang, Qinhe Pan*

Key Laboratory of Advanced Materials of Tropical Island Resources, Ministry of Education, School of Chemistry and Chemical Engineering, Hainan University, Haikou 570228, Hainan, China.

***Correspondence to:** Dr. Xiaojun Zhao, Prof. Qinhe Pan, Key Laboratory of Advanced Materials of Tropical Island Resources, Ministry of Education, School of Chemistry and Chemical Engineering, Hainan University, 58 Renmin Avenue, Haikou 570228, Hainan, China. E-mail: xiaojunzhao2013@163.com; panqinhe@163.com

How to cite this article: Lin Y, Gan L, Zhao X, Che G, Wang S, Pan Q. Facile synthesis of Ag/AgCl/PAF-54 heterojunction photocatalysts for TC degradation. *Chem Synth* 2024;4:32. https://dx.doi.org/10.20517/cs.2024.17

Received: 3 Feb 2024 **First Decision:** 23 Apr 2024 **Revised:** 2 May 2024 **Accepted:** 20 May 2024 **Published:** 11 Jun 2024

Academic Editor: Jin Xie **Copy Editor:** Pei-Yun Wang **Production Editor:** Pei-Yun Wang

Abstract

Photocatalysis plays an increasingly important role in the field of water treatment. Among the catalysts, Ag nanoparticles (NPs), a type of noble metal NP, show extraordinary potential for photocatalysis. Nevertheless, the aggregation caused by high surface energy limits their applications. The simple synthesis of Ag NPs with uniform size remains a challenge. In this work, a nitrogen-rich porous organic polymer (POP) with reduction ability, porous aromatic framework (PAF)-54, was chosen as the carrier for the *in-situ* synthesis of Ag NPs. By virtue of the reducing framework of PAF-54 and the formation of the AgCl/PAF-54 heterojunction, the *in-situ* reduction of Ag(I) was realized, and thus Ag NPs with the particle size of 20-25 nm were uniformly distributed on PAF-54, which exhibit a strong localized surface plasmon resonance (LSPR) effect. Furthermore, the Ag/AgCl/PAF-54 heterojunction effectively suppresses the recombination of photogenerated electrons and holes, leading to the enhanced photocatalytic ability of the composite material. Even with a small catalyst dosage, rapid tetracycline (TC) degradation can be achieved, and the degradation rate of TC reached 94.8% in 30 min. This study offers a facilitated approach for fabricating Ag-based POP composites with superior photocatalytic properties.

Keywords: Ag NPs, PAF-54, photocatalysis, localized surface plasmon resonance, heterojunction

INTRODUCTION

In recent years, the rise of organic pollutants, such as antibiotics and pesticides, has posed a growing threat

to ecosystems and human health[1-3]. Photocatalysis, a green and sustainable catalytic technology, holds promise in addressing this challenge[4-8]. Among the various photocatalysts, noble metal nanomaterials have garnered significant attention due to their potentially outstanding photocatalytic degradation activity for toxic organic pollutants[9]. On the one hand, their excellent electrical conductivity enables them to act as an electron sink to promote charge carrier separation. On the other hand, the noble metal nanoparticles (NPs) may induce localized surface plasmon resonance (LSPR) effect to enhance the solar energy conversion efficiency[10,11]. In particular, Ag NPs have been widely investigated as high-performance photocatalysts due to their relatively low cost, strong LSPR effect, and tunability[12]. When a small particle size of around 25 nm of Ag NPs is optimized and their uniform distribution is adjusted, a significant LSPR effect is observed, greatly enhancing the photocatalytic activity[13]. However, the high surface energy of Ag NPs promotes aggregation, undermining their catalytic activity and efficient use[14].

To address this problem, porous materials, such as porous silica[15], zeolite[16], carbon-based materials[17], polymers[18], and metal-organic frameworks[19], are often used as supports to anchor the metal NPs. This approach ensures the uniform distribution of NPs, enhancing catalytic activity, stability and reusability[20,21]. Porous organic polymers (POPs), a novel lightweight porous material with stable backbone structure, ultra-high specific surface area, and tunable pore functionality[22-25], are also suitable candidates as metal NP supports[26,27]. The tunable groups in the POP structure can act as anchoring sites for metal NPs, effectively preventing their aggregation[28-30]. In addition, the abundant porous structure facilitates the diffusion and contact of organic pollutant molecules with metal NPs on the catalyst surface. A common method for preparing Ag NPs and POPs composites involves adsorbing Ag^+ on the POP carrier and then introducing a reducing agent such as $NaBH_4$[31], polyvinylpyrrolidone (PVP)[32] or hydroxylamine hydrochloride[33] to form Ag NPs. However, during the reduction process of Ag^+ on the carrier, precise control of the amount and rate of the reducing agent is crucial to ensure an appropriate reaction rate, in order to avoid significant aggregation of the reduced Ag^0. This not only increases the cost and complexity of Ag NP-based material synthesis but may also lead to inadequate anchoring of Ag NPs on the POP carrier. In addition, under ultraviolet (UV) light in the presence of halogens, it is possible to induce the formation of AgX which can further undergo photoreduction to Ag^0[34]. However, the morphology of Ag NPs prepared by this method is typically a pending issue. In order to prepare well-distributed Ag-based photocatalysts, it is necessary to develop a facile method.

Nitrogen-rich POPs offer a large number of N atoms that can serve as both adsorption sites for Ag^+ and anchoring sites for Ag NPs[35]. What is more, according to the literature, some nitrogen-rich POPs possess reducing properties, and their N-containing functional groups can reduce metal ions such as Ag and Au[36,37]. Therefore, by selecting suitable nitrogen-rich POPs as both a carrier and reducing agent to adsorb Ag^+ and undergo moderate *in-situ* reduction, it is anticipated that Ag NPs with uniform sizes and distributions will be formed, ultimately maximizing the photocatalytic efficiency and usability.

Here, in order to obtain spatially highly dispersed Ag NPs, we selected porous aromatic framework (PAF)-54, a nitrogen-rich POP with reduction framework, as a carrier capable of anchoring and *in-situ* reduction of Ag(I). The Ag/AgCl/PAF-54 composite was synthesized by a simple one-step "post-synthesis" strategy. On the one hand, the abundant nitrogen elements in the PAF-54 framework can reduce the adsorbed Ag^+ and anchor it securely. On the other hand, the Cl elements within PAF-54 also promote the adsorption of Ag^+ and form an AgCl/PAF-54 heterojunction, further accelerating the photocatalytic decomposition of AgCl[38]. As expected, Ag NPs with uniform size (20-25 nm) are uniformly distributed in the prepared composite and exhibit a strong LSPR effect, which greatly improves the visible light utilization of the composite. In addition, the ternary heterojunction formed by Ag NPs, PAF-54 and AgCl effectively hinders

the recombination of holes with photogenerated electrons, leading to exceptional photocatalytic performance[39]. Notably, a degradation efficiency (DE) of 94.8% for tetracycline (TC) was achieved within 25 min. This study provides a new perspective for fabricating Ag NP-based catalysts and opens new avenues for designing POP materials to treat organic pollutants.

EXPERIMENTAL

Preparation of PAF-54

As reported in the literature[40], 45 mL of dimethyl sulfoxide (DMSO) was used to dissolve 829.8 mg of cyanogen chloride (4.5 mmol) (solution 1). Subsequently, solution 1 was gradually added to solution 2, which consisted of 45 mL of DMSO dissolved in 567.5 mg of melamine (4.5 mmol) and 0.6 mL of triethylamine (EtN_3). The reaction system is then heated at 150 °C for 24 h under nitrogen atmosphere. After cooling to room temperature, the resulting egg-white precipitate was filtered and thoroughly washed with excess DMSO, H_2O, and EtOH, then dried under vacuum. Finally, the white lumpy solid was ground into powder.

Preparation of photocatalysis

Preparation of Ag/AgCl/PAF-54

First, 50.0 mg of $AgNO_3$ was dissolved in 10.0 mL of deionized water, and 50.0 mg of PAF-54 powder was added and stirred under natural light for one day. The solid product was collected by centrifugation, washed five times with deionized water and dried under vacuum at room temperature to give Ag/AgCl/PAF-54(1:1). When the amount of $AgNO_3$ was 10.0 and 100.0 mg, Ag/AgCl/PAF-54(1:5) and Ag/AgCl/PAF-54(2:1) were obtained, respectively.

Preparation of AgCl/PAF-54

First, 50.0 mg $AgNO_3$ was dissolved in 10.0 mL of deionized water, respectively. Then, 50.0 mg PAF-54 powder was added and stirred for one day in the dark. The solid product was collected by centrifugation, washed five times with deionized water and dried at room temperature under vacuum.

Preparation of Ag/AgCl/PAF-54($NaBH_4$)

In order to compare the superiority of this strategy, Ag NPs were obtained by reduction using $NaBH_4$. This was done as follows: firstly, PAF-54 was added to a stoichiometric $AgNO_3$ solution (consistent with the Ag loading of the above samples, 13.8%), and after adsorption under dark for 24 h, 1.5 mL $NaBH_4$ (3 mM) was added. Then, continue stirring under dark light for 12 h. After washing with deionized water and ethanol three times, collect by centrifugation and dry under vacuum at room temperature for 24 h to obtain Ag/AgCl/PAF-54($NaBH_4$).

Evaluation of the prepared photocatalysts

Degradation of TC by irradiation with a 300 W Xe lamp with a 420 nm cut filter was used to assess its photocatalytic efficiency. In a type procedure, 10 mg of the prepared samples were put into 50.0 mL of TC aqueous solution (10 mg/L). Before photocatalysis, the solution is stirred in dark light for 30 min to reach adsorption equilibrium. During the reaction, about 1 mL of the suspension was withdrawn from the mixture with a syringe and filtered through a 0.45 μm membrane. To analyze the change in TC concentration, the absorbance of the filtrate at 357 nm was monitored using a UV-visible (vis) spectrophotometer. Intermediates produced during TC degradation were further analyzed on a high-performance liquid chromatography-mass spectrometry (HPLC-MS) system.

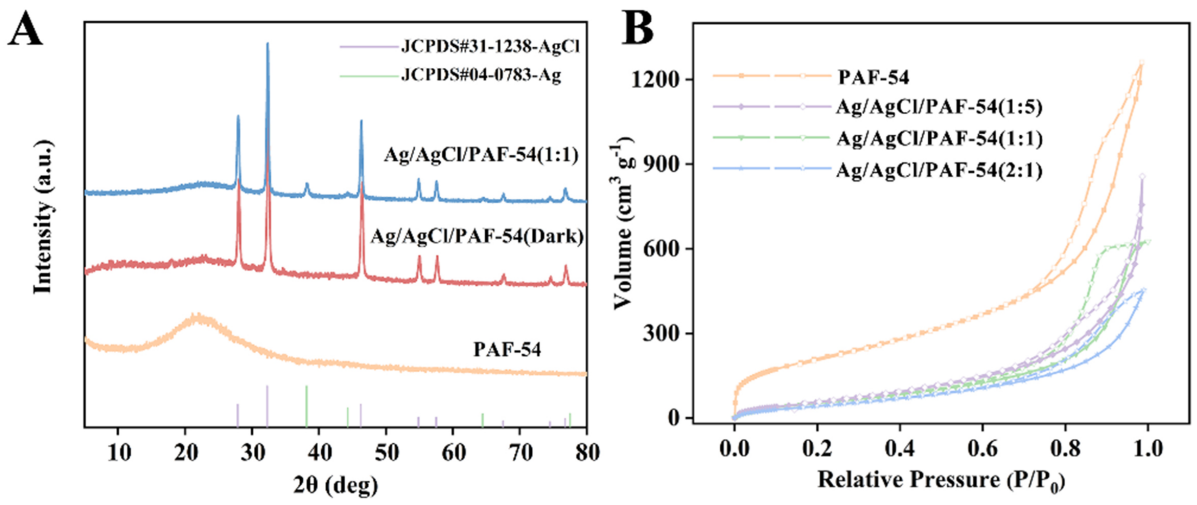

Figure 1. (A) PXRD pattern of PAF-54, Ag/AgCl/PAF-54(1:1) and Ag/AgCl/PAF-54(Dark); (B) N_2 adsorption-desorption isotherms of the synthesized samples. PXRD: Powder X-ray diffraction; PAF: porous aromatic framework.

The DE and total organic carbon (TOC) were calculated by

$$\text{DE or TOC} = \frac{C_0 - C_t}{C_0} \times 100\% \quad (1)$$

where C_0 is the concentration of TC or TOC before degradation; C_t is the concentration of TC or TOC at moment (t).

RESULTS AND DISCUSSION

Characterization of the prepared photocatalyst

First, the successful preparation of the carrier PAF-54 was confirmed by Fourier Transform Infrared Spectroscopy (FTIR) and Carbon-13 Cross Polarization Magic Angle Spinning Nuclear Magnetic Resonance (^{13}C CPMAS NMR) [Supplementary Figure 1]. Through a simple one-step "post-synthesis" strategy, Ag NPs were formed *in situ* on the PAF. As shown in Figure 1A, the absence of significant diffraction peaks in the powder X-ray diffraction (PXRD) pattern of PAF-54 indicates that PAF-54 is an amorphous network. After loading Ag NPs, three diffraction peaks at 38.1°, 44.3° and 64.1° correspond to Ag^0, implying the formation of Ag^0[41] and other samples [Supplementary Figure 2]. Besides, diffraction peaks (27.8°, 32.2°, 46.2°, 54.8°, 57.5°, 67.5°, and 74.5°) belonging to AgCl were also clearly observed, which may be attributed to the introduction of elemental Cl during the PAF-54 synthesis. After loading with Ag NPs, the specific surface of the composites decreased rapidly and further diminished with rising $AgNO_3$ dosage, which may be caused by the clogging of Ag NPs in the pores [Figure 1B]. Fortunately, the composites still exhibit a high specific surface area and rich pore structure [Supplementary Figure 3 and Supplementary Table 1], which was beneficial for exposing active sites in the catalytic process and facilitating mass transfer[42]. Moreover, the specific surface of the composites decreased gradually with the increase of $AgNO_3$ dosage.

To further confirm that Ag NPs are anchored to the PAF-54 carrier, high-resolution transmission electron microscopy (HRTEM) for microscopic morphology was conducted. As shown in Figure 2A, Ag NPs with a size of about 20-25 nm were uniformly distributed on the carrier. These NPs exhibited an inter-planar spacing of 0.223 nm, consistent with the spacing of the (1 1 1) lattice plane of the Ag crystal [Figure 2B].

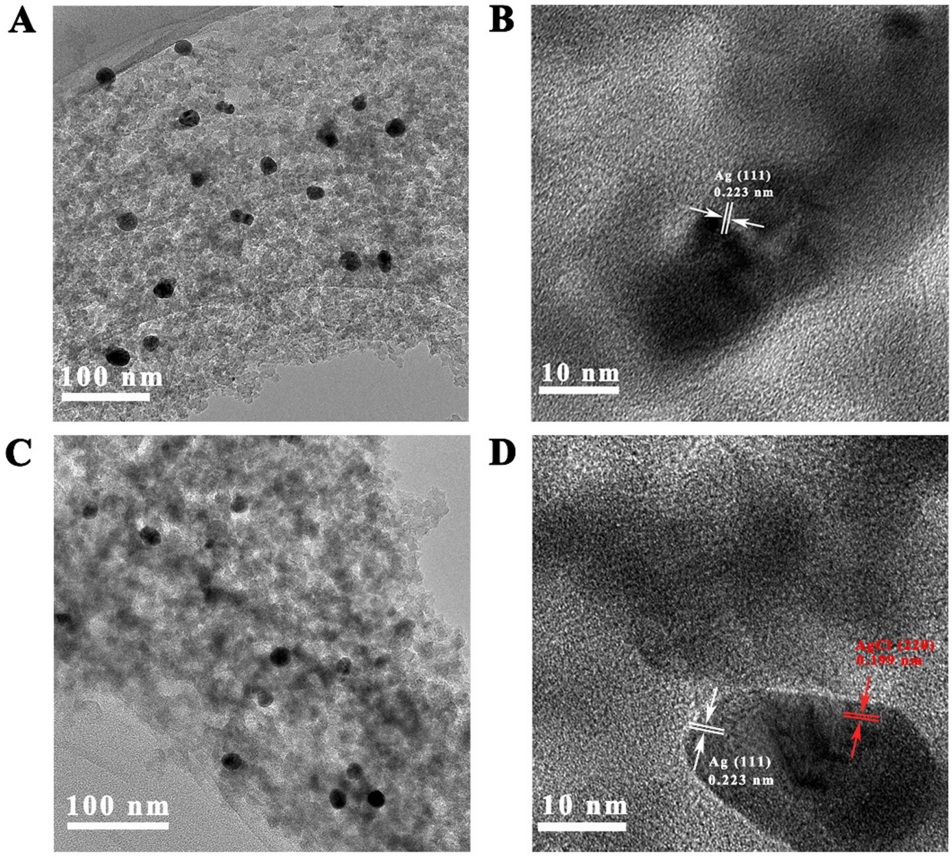

Figure 2. TEM of (A) Ag/AgCl/PAF-54(1:1) and (C) Ag/AgCl/PAF-54(Dark). HRTEM of (B) Ag/AgCl/PAF-54(1:1) and (D) Ag/AgCl/PAF-54(Dark). TEM: Transmission electron microscopy; PAF: porous aromatic framework; HRTEM: high-resolution transmission electron microscopy.

Besides, comparing the total X-ray photoelectron spectroscopy (XPS) spectra before and after loading, it is obvious that an extra peak feature belongs to Ag [Supplementary Figure 4A]. As shown in the Figure 3A, the Ag 3d XPS spectra of the Ag/AgCl/PAF-54 composites could be fitted into four peaks at 368.36, 369.20, 374.46 and 375.20 eV, which could be corresponded to Ag^+ $3d_{5/2}$, Ag^0 $3d_{5/2}$, Ag^+ $3d_{3/2}$, and Ag^0 $3d_{3/2}$, respectively. This further demonstrated the successful introduction of Ag and AgCl components into the PAF-54 carrier. In addition, in the XPS spectra of N 1s [Supplementary Figure 4B and C], the binding energies of C=N-C and N-H were significantly shifted (398.51 ⟶ 399.75, 399.80 ⟶ 400.05 eV, respectively) after Ag NP loading, indicating strong interactions between the N atoms of PAF-54 and the incorporated metal centers. The high content of N (62.70 wt%) played an important role in the adsorption of Ag^+ and limiting and immobilizing the growth of Ag NPs.

Analysis of Ag^0 formation

Ag^0 may be formed by

$$AgCl + e^- = Ag^0 + Cl^- \quad (2)$$

$$Ag^+ + e^- = Ag^0 \quad (3)$$

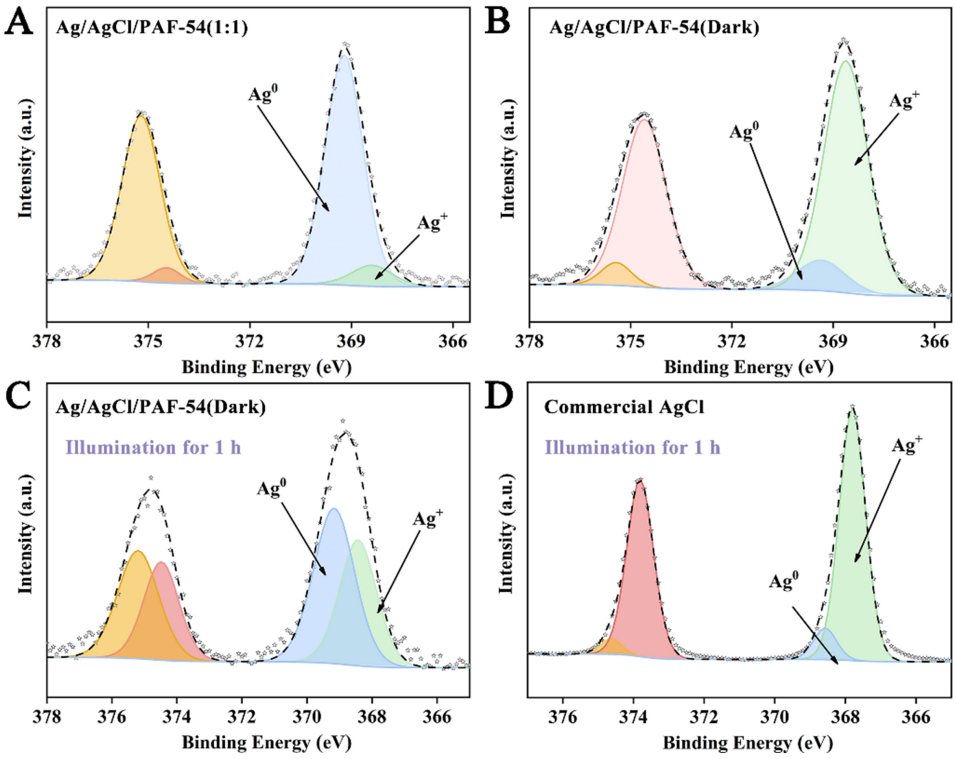

Figure 3. Ag 3d of Ag/AgCl/PAF-54(1:1) in (A) natural light and (B) dark. Ag 3d of (C) Ag/AgCl/PAF-54 and (D) Ag/AgCl in natural light for 1 h. PAF: Porous aromatic framework.

In order to investigate the mechanism of *in-situ* reduction of Ag^0 in detail, the preparation process was carried out in the dark, and the product was used for comparison. Supplementary Figure 5 shows a notable color difference between the samples prepared in natural light and those prepared in darkness, possibly due to the difference in the number of Ag NPs. The differences between the two samples were further analyzed using PXRD, HRTEM, and XPS. Firstly, as shown in Figure 1A, the diffraction peaks attributed to Ag^0 in Ag/AgCl/PAF-54(Dark) are less pronounced than Ag/AgCl/PAF-54(1:1), which may be caused by too little Ag^0 content. For the sample obtained under natural light, anchored Ag^0 is an absolutely dominant form. However, for Ag/AgCl/PAF-54(Dark), the Ag element primarily exists in the forms of deposited AgCl and adsorbed Ag^+ [Figure 3B]. The XPS peaks of Ag 3d of Ag/AgCl/PAF-54(Dark) are analyzed. The fitting peaks at 368.66 and 374.67 eV belong to Ag^+, and those at 369.22 and 376.35 belong to Ag^0. The group of PAF-54 on the surface participated in the redox reaction during the Ag^+ adsorption process, and part of the Ag^+ was reduced to Ag^0. It has been reported in the literature that functional groups containing nitrogen can reduce Ag^+[20,37]. In addition, the presence of Ag^0 was also observed in transmission electron microscopy (TEM) and HRTEM images [Figure 2C and D], so these can fully prove that PAF-54 can reduce Ag^0 *in situ*. Moreover, PAF-54 also contributes to the formation of AgCl and its conversion to Ag^0. The uniformly distributed Cl element in PAF-54 can accumulate Ag^+ and form AgCl NPs. And it is possible to form an AgCl/PAF-54 heterojunction, which can accelerate the photoreduction process of AgCl. The AgCl-to-Ag photoreduction rate of the above AgCl/PAF-54 and pure AgCl was explored to verify this. As shown in Figure 3C and D, after one hour of exposure to natural light, the proportion of Ag^0 (56.88%) in the product of AgCl/PAF-54 is significantly higher than that (7.81%) in the product of AgCl, indicating that the presence of PAF-54 indeed favors the conversion of AgCl to Ag. For the PAF-54 carrier, on the one hand, by the strong soft-soft interactions, the N soft donor atoms act as anchoring sites to adsorb Ag^+, which can reduce Ag *in situ* [Equation (2)] and further anchor Ag^0. On the other hand, the Cl element in PAF-54 can further

promote the adsorption of Ag^+, forming an AgCl/PAF-54 heterojunction, which promotes the photoreduction of AgCl to form Ag^0 [Equation (3)]. The Ag NPs reduced *in situ* by the above two paths feature uniform particle size and distribution, and also form a ternary heterojunction with AgCl and PAF-54. Therefore, the composite may have great potential in photocatalysis.

Photocatalytic performances

Type and usage of photocatalysts

The photocatalytic performance of Ag/AgCl/PAF-54 was evaluated with TC as the degradation target [Figure 4]. As shown in Supplementary Figure 6A, the adsorption of TC reached equilibrium quickly (30 min) in the dark due to the rich pore structure of the photocatalysts, which may also facilitate the subsequent photocatalysis. As expected, the photocatalytic performance was significantly enhanced upon introducing Ag and AgCl. When the dosage of $AgNO_3$ was consistent with that of PAF-54, Ag/AgCl/PAF-54(1:1) showed the highest photocatalytic activity, with a fast TC DE of 94.8% within 25 min and a TOC removal efficiency of 60.2%. Therefore, this sample was used for all subsequent experiments. The photocatalytic degradation spectrum of Ag/AgCl/PAF-54(1:1) is shown in Supplementary Figure 6B. The UV absorption peak of TC did not change during the 30 min of dark light adsorption, indicating that only the adsorption process was performed in the dark. After the light exposure, the peaks exhibited changes, possibly due to the appearance of intermediates of TC decomposition. Figure 4B shows that the efficiency of TC degradation increased from 89.7% to 94.8% as the dosage of Ag/AgCl/PAF-54(1:1) was elevated from 5 to 10 mg. However, when further increased to 15 mg, the removal rate did not significantly improve. This may be due to the excess sample in the solution obscuring and scattering photon absorption.

Effect of pH

To evaluate the influence of pH on TC degradation, the solution pH was adapted to 2.5-9.5 for photocatalytic experiments. The PXRD pattern of Ag/AgCl/PAF-54(1:1) did not reveal significant changes in this pH range, indicating the strong stability of the photocatalyst at different pH [Supplementary Figure 7]. As shown in Figure 4C, the pH change affected the adsorption of TC by Ag/AgCl/PAF-54(1:1), which, in turn, affected the subsequent photocatalysis. The TC removal efficiency enhanced with increasing pH and reached the highest value at pH = 8.5. This was possibly due to the electrostatic interaction between TC and photocatalysts, which affects the adsorption probably. As reported in the literature, TC presents diverse forms in aqueous solutions at varying pH, including cationic species TCH_3^+ (pH < 3.3), zwitterionic species TCH_2 (3.3 < pH < 7.7) and anionic species TCH^- or TC_2^- (pH > 7.7)[34]. The surface charge characteristics of Ag/AgCl/PAF-54(1:1) were revealed by zeta potential measurements [Supplementary Figure 8]. The surface charge decreases gradually with rising pH and reaches the point of zero charge at a pH of about 9.5. Therefore, when in an acidic environment, the catalyst is protonated and the positive charge attached to the surface creates electrostatic repulsion with the TC, which is also a cation, leading to a decrease in adsorption. When in a strongly alkaline environment, two negatively charged substances undergo electrostatic repulsion. When the pH was 8.5, a large number of TC anions existed in the solution, while Ag/AgCl/PAF-54(1:1) remained positively charged and, therefore, had a strong adsorption capacity for TC. However, most of the actual water samples are weakly alkaline. Considering the practical application, the pH of subsequent experiments was adjusted to 7.5. Under this condition, rapid and excellent TC degradation can be achieved with a lower catalyst dosage, which is superior to the majority of the reported Ag-based photocatalysts [Table 1].

Comparison with $NaBH_4$-reduced sample

When the strong reducing agent $NaBH_4$ was used to prepare Ag NPs, the Ag NPs were obtained of inconsistent sizes and prone to agglomeration [Supplementary Figures 9 and 10]. Compared with the composites reduced *in situ* by PAF-54, the photocatalytic performance was greatly weakened, and the DE

Table 1. The photocatalytic degradation of TC by different Ag-base photocatalysts reported in literature

Catalysts	Concentration (mg/L)	Dosage (g/L)	Time (min)	Removal efficiency	TOC	Ref.
$Ag/Ag_2CO_3/BiVO_4$	20	1.0	150	94.9%	N.A.	[43]
Ag-g-C_3N_4	20	0.5	120	99.1%	81.1%	[44]
Ag@HNT	10	0.4	80	95.8%	N.A.	[45]
$Ag/AgIn_5S_8$	10	0.3	120	95.3%	N.A.	[46]
$BPQDs/Ag/TiO_2$	10	N.A.	90	92.4%	71.7%	[47]
Ag@MOF-525	10	0.4	200	81.0%	N.A.	[48]
Ag/AgCl/BiOCl	20	0.375	60	83.0%	N.A.	[49]
$Bi_2WO_6/BiOI/Ag$	20	1.0	120	96.2%	33.2%	[50]
COF TzDa/Ag/AgBr	10	0.4	30	80.0%	N.A.	[34]
$PI/TiO_2/Ag$-0.07	5	N.A.	120	93.1%	N.A.	[51]
Ag/Cl-CN	20	0.5	120	90.2%	70.2%	[52]
Ag/AgCl/PAF-54	10	0.1	30	90.0%	52.7%	This work
Ag/AgCl/PAF-54	10	0.2	25	94.8%	60.2%	This work

TC: Tetracycline; TOC: total organic carbon; N.A.: not available; COF: covalent organic framework; PAF: porous aromatic framework.

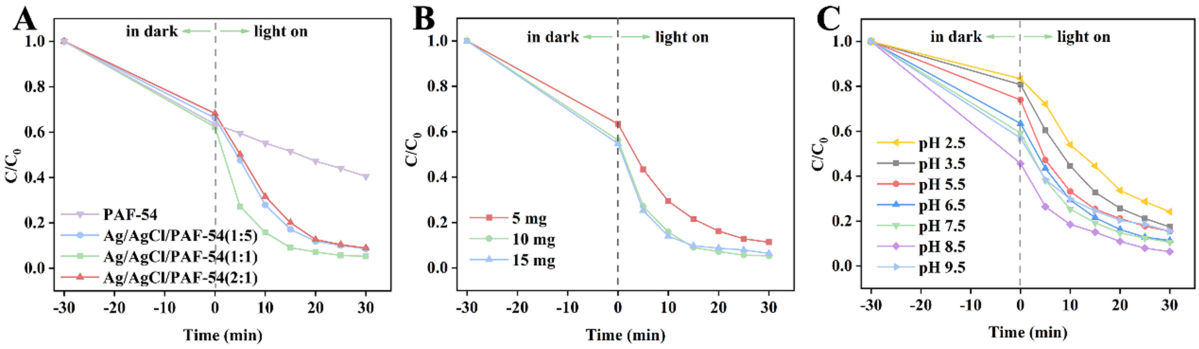

Figure 4. (A) Degradation of TC by various photocatalysts under visible light. Effects of (B) catalyst dosage and (C) pH on TC degradation. TC: Tetracycline.

could only reach 66.8% within 25 min [Supplementary Figure 11]. This is because the ununiformly distributed Ag NPs diminish the LSPR effect and the exposure of the catalytically active sites and reduce the mass transfer process between TC and Ag. In addition, agglomerated Ag increases the probability of complexation of photogenerated electrons and holes, thus weakening its photocatalytic ability.

Photocatalyst recyclability and universality

In addition, to assess the practical application of Ag/AgCl/PAF-54(1:1) for antibiotic degradation in real water samples, photocatalytic tests were performed using pool water, piped water, river water and seawater[53]. The results, as shown in Supplementary Figure 12A, indicate that the different aqueous environments had very little effect on the TC DE. This suggests that the catalyst has great potential for practical application in treating TC-contaminated water. Besides, the photocatalytic degradation efficiencies could reach more than 80% for other TC antibiotics [Supplementary Figure 12B]. The excellent versatility of Ag/AgCl/PAF-54(1:1) enables it to handle complex situations in real environments. And its photocatalytic stability was investigated [Supplementary Figure 12C]. No serious deactivation was observed during the three cycles, and there were no significant changes in the FTIR and XRD pattern of the catalysts before and after the reaction [Supplementary Figure 13], confirming its stability. A small decrease in TC removal efficiency could be attributed to the loss of photocatalyst or leaching of Ag^0 (1.13%).

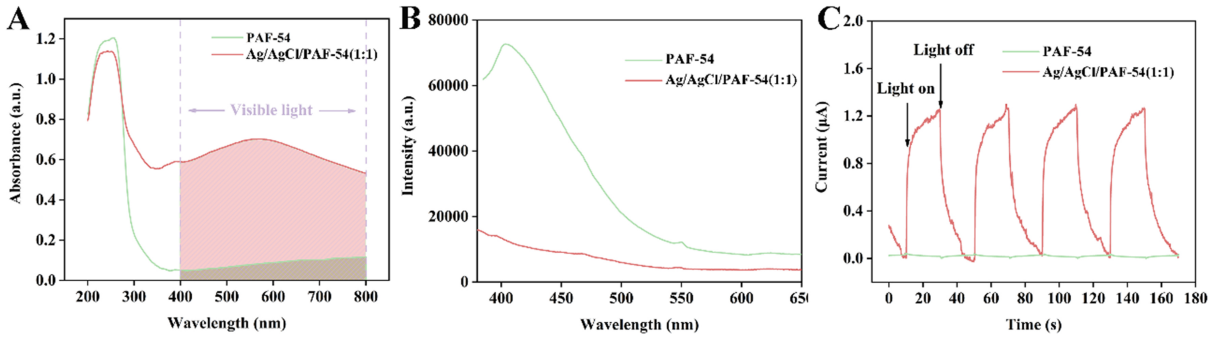

Figure 5. (A) UV-vis di use reflection spectra; (B) PL emission spectra; and (C) Transient photocurrent response of PAF-54, Ag/AgCl/PAF-54(1:1). UV: Ultraviolet; PL: photoluminescence; PAF: porous aromatic framework.

Optical and photo-electrochemical properties

The optical properties of the catalyst are an important factor influencing the activity of high-performance photocatalysis. Therefore, the optical properties of the resulting photocatalyst were analyzed by UV-vis diffuse reflectance spectroscopy (DRS). Compared to PAF-54, the prepared composite catalysts showed a significant enhancement of visible light absorption [Figure 5A]. This increase was attributed to the LSPR effect of Ag NPs, which effectively enhances the light absorption and reduces the bandgap of the prepared photocatalysts. This optimization enhances the efficiency of solar energy utilization and generates more photogenerated electron-hole pairs, thereby enhancing the efficiency of the photocatalytic process. Additionally, we compared the fluorescence intensities of the materials before and after loading [Figure 5B], and it was clearly found that after loading, the fluorescence intensity of the composites decreased dramatically, which implies that the recombination rate of the photogenerated carriers was reduced. Therefore, it is favorable for producing active substances in the photocatalytic process[54]. In addition, the charge transfer ability of Ag/AgCl/PAF-54 was further investigated by evaluating its photocurrent response. As shown in Figure 5C, Ag/AgCl/PAF-54(1:1) exhibits a strong photocurrent, much larger than that of PAF-54. Besides, electrochemical impedance spectroscopy (EIS) was used to explain the light-induced separation efficiency of e^- and h^+ carriers. As shown in Supplementary Figure 14, after loading Ag NPs, the impedance of the composite is significantly reduced, indicating that the photogenerated carrier transfer speed at the catalyst interface is increased. On the one hand, introducing Ag NPs with excellent electrical conductivity can act as an electron sink to promote the separation of carriers. On the other hand, the prepared heterojunction accelerates the separation of holes and electrons. Therefore, the photocatalytic ability can be greatly enhanced.

Possible photodegradation mechanisms

In the photocatalytic progress, active substances, such as holes (h^+), superoxide ($\bullet O^{2-}$), and hydroxyl radicals ($\bullet$OH), play crucial roles in TC degradation. Therefore, scavenging experiments were performed using ethylenediaminetetraacetic acid (EDTA), 2,2,6,6-tetramethylpiperidine-1-oxyl (TEMPO), and isopropanol (IPA) as h^+, $\bullet O^{2-}$, and $\bullet$OH scavengers, respectively. As shown in Figure 6A, EDTA had a significant inhibitory effect on TC degradation (94.8 $\longrightarrow$ 7.2%), and with the addition of TEMPO, the DE decreased to 48.8%. Therefore, h^+ and $\bullet O^{2-}$ were proved to be the main reactive substances involved in TC degradation. The effect of IPA on the degradation of TC by Ag/AgCl/PAF-54 was negligible. In addition, As shown in Figure 6B and C, no visible free radicals were detected in the dark. As the light exposure period extended, the $\bullet O^{2-}$ signals increased noticeably, suggesting that more free radicals were created during the process. Together with the free radical scavenging experiments, these results suggest that h^+ and $\bullet O^{2-}$ play a greater role in TC degradation.

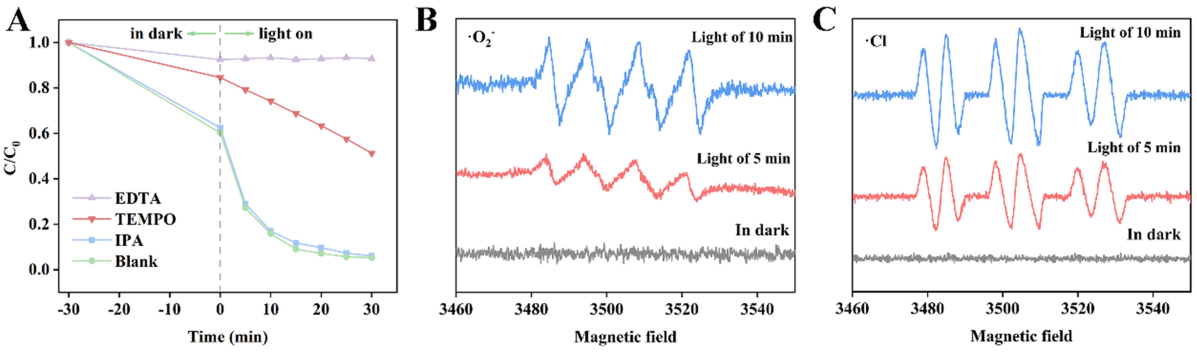

Figure 6. (A) Inhibition of different scavengers on TC degradation; ESR spectra of (B) DMPO-•O_2^- and (C) PBN-•Cl. TC: Tetracycline; ESR: electron spin resonance; DMPO: 5, 5-dimethyl-1-pyrroline-N-oxide; PBN: N-tert-butyl-alpha-phenylnitrone.

To further understand the mechanism of photocatalysis, the flat band potential (E_{FB}) of PAF-54 was calculated using the Mott-Schottky diagram, resulting in a value of -0.47 V [*vs.* Normalized Hydrogen Electrode (NHE)]. In general, the conduction band (E_{CB}) of n-type semiconductors is about 0.1 V more negative than the E_{FB}. Thus, PAF-54 has a CB of -0.57 V (*vs.* NHE). According to the UV-vis DRS [Supplementary Figure 15], its band gap (Eg) is 4.35 V (*vs.* NHE), which corresponds to a valence band (E_{VB}) of 3.78 V (*vs.* NHE). It can be observed that PAF-54 has a broad bandgap, making it difficult to be directly excited by visible light. Due to the effect of LSPR and dipole characteristics of Ag NPs, Ag NPs can absorb visible light and convert the absorbed photons into electrons and holes effectively. The generated hot electrons can transfer to the conduction band of PAF-54, generating •O_2^- (O_2/•O_2^- -0.33 eV *vs.* NHE) and degrading TC into smaller molecules. PAF-54 facilitates the rapid transfer of photo-generated electrons, resulting in lower recombination rates and enhanced photocatalytic activity. In addition, the remaining holes on the surface of Ag NPs can directly degrade TC. Some of these holes can also transfer to the surface of AgCl, oxidizing Cl^- into •Cl active radicals [Figure 6C], which may further degrade TC [Figure 7][55,56].

Potential pathways of TC degradation

Liquid chromatography tandem mass spectrometry (LC-MS) was utilized to detect the degradation products of TC to explore the degradation pathways and mechanisms. Additionally, Supplementary Table 2 overviews the structural data, mass spectrometry (MS) spectra, and the primary potential intermediates. Drawing from related reports, we proposed two possible pathways for the photocatalytic degradation of TC by Ag/AgCl/PAF-54 [Figure 8][34]. In pathway 1, the decomposition of TC is mainly induced by hydroxylation. Firstly, TC forms P1 (m/z 461.11) by hydroxylation, which is then further oxidized to P2 (m/z 478.15) by reactive oxygen species. Subsequently, P2 is attacked by active radicals to form the dehydration product P4 (m/z 459.14). In addition, P1 can be converted to P3 (m/z 433.16) by direct N-dealkylation and then be dehydrated by reacting with reactive radicals to produce P5 (m/z 415.15). Pathway 2 mainly involves the N-methyl detachment. Firstly, TC forms P6 (m/z 432.23) by losing the N-methyl group and then undergoes further loss to form P8 (m/z 416.28). If a H_2O molecule is lost, P7 (m/z 413.13) is formed. Afterward, the above intermediates are oxidized by reactive substances, resulting in ring opening and forming other small organic molecules. Ultimately, these intermediates are fully oxidized into smaller molecules such as CO_2, H_2O and NH_3.

CONCLUSIONS

To sum up, uniformly distributed and stable Ag NPs anchored in PAF-54 were generated *in situ* using a simple synthetic method. On the one hand, due to the reducing property of a large number of nitrogen-containing functional groups in PAF-54, adsorbed Ag^+ was reduced to Ag^0. On the other hand, the Cl

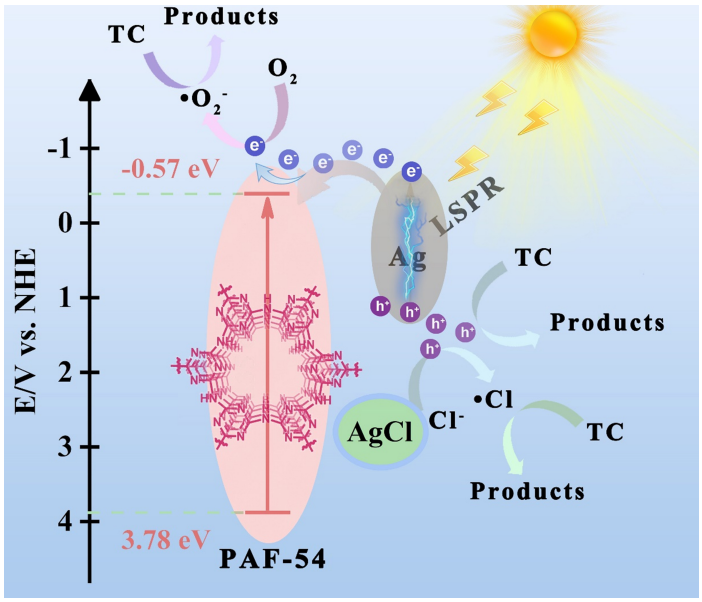

Figure 7. Mechanism of photodegradation TC on Ag/AgCl/PAF-54. TC: Tetracycline; PAF: porous aromatic framework.

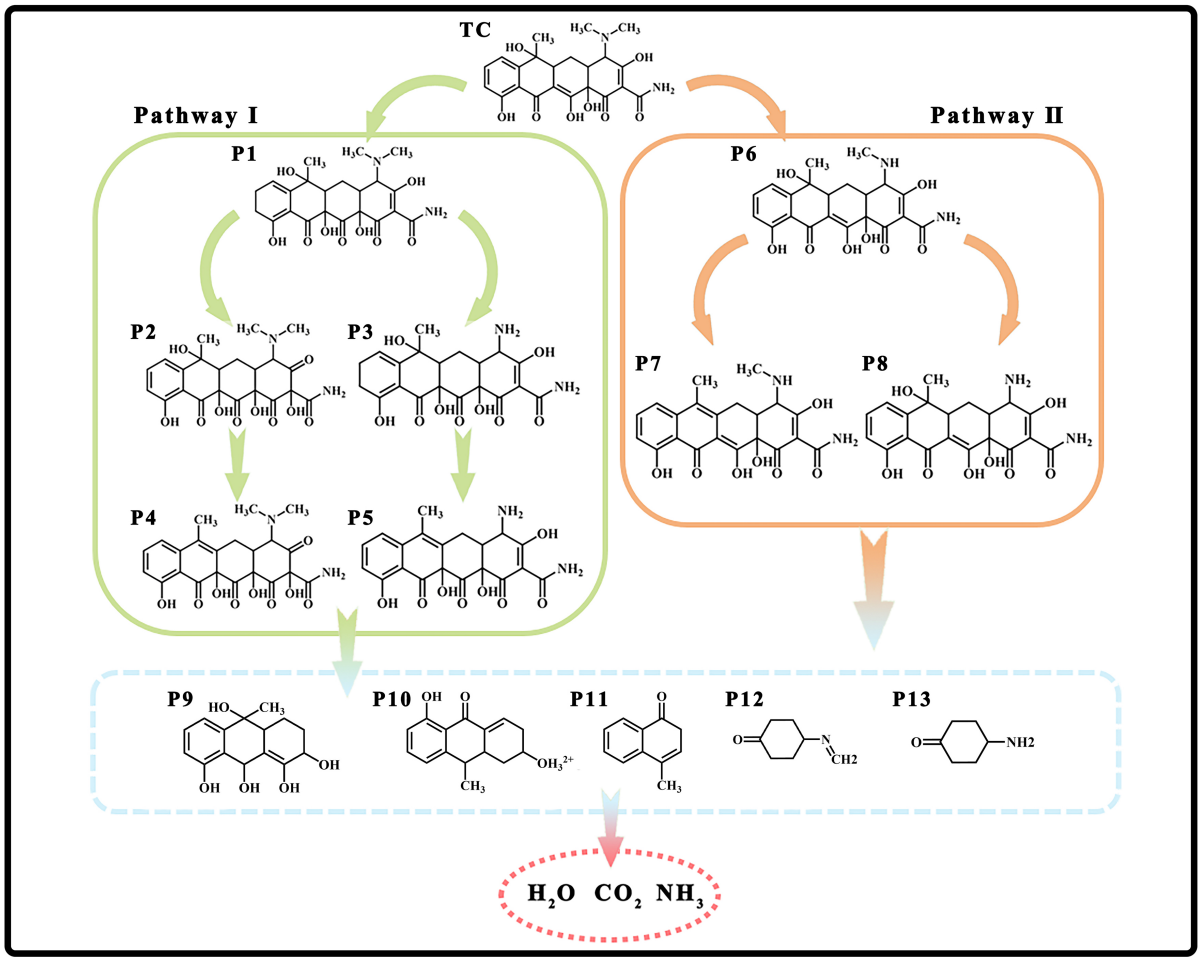

Figure 8. Proposed photodecomposition process of TC. TC: Tetracycline.

element in PAF-54 also promotes the adsorption of Ag^+ and the formation of AgCl. PAF-54 may be complex with the attached AgCl to form heterojunctions, which further accelerates the photocatalytic decomposition of AgCl. Due to the well-dispersed and appropriately sized particles of Ag NPs, the photocatalyst exhibits a strong LSPR effect, which enhances the utilization of visible light for the composites. In addition, the formation of ternary heterojunction with PAF-54, Ag and AgCl effectively inhibits the recombination of holes with photogenerated electrons. Therefore, Ag/AgCl/PAF-54 exhibits excellent TC photodegradation performance, enabling rapid and effective TC degradation with a low catalyst dosage. More importantly, this study provides a simple strategy for fabricating Ag-based photocatalysts.

DECLARATIONS

Authors' contributions

Supervised the Project and revised the manuscript: Zhao X, Pan Q

Responsible for data collection, analysis and wrote the original manuscript: Lin Y, Gan L, Che G, Wang S

Availability of data and materials

Experimental details and supporting data can be found in Supplementary Materials.

Financial support and sponsorship

This work was supported by Hainan Provincial Natural Science Foundation of China (220MS005), the National Natural Science Foundation of China (22361017), the Innovation Platform for Academicians of Hainan Province, the Specific Research Fund of the Innovation Platform for Academicians of Hainan Province (YSPTZX202321), and the International Science & Technology Cooperation Program of Hainan Province (No. GHYF2022006).

Conflicts of interest

All authors declared that there are no conflicts of interest.

Ethical approval and consent to participate

Not applicable.

Consent for publication

Not applicable.

REFERENCES

1. El Khawaja R, Veerapandian SKP, Bitar R, et al. Boosting VOCs elimination by coupling different techniques. *Chem Synth* 2022;2:13. DOI
2. Che G, Yang W, Luo J, Li M, Li X, Pan Q. Efficient adsorption and photocatalysis over a photorenewable uranyl-organic framework for removal of diquat herbicide. *Sep Purif Technol* 2024;334:126126. DOI
3. Aghajani Z, Hosseinpour-mashkani SM. Design novel $Ce(MoO_4)_2$@TiO_2*n–n* heterostructures: enhancement photodegradation of toxic dyes. *J Mater Sci Mater Electron* 2020;31:6593-606. DOI
4. Li Y, Zhang D, Qiao W, et al. Nanostructured heterogeneous photocatalyst materials for green synthesis of valuable chemicals. *Chem Synth* 2022;2:9. DOI
5. Feng JQ, Li L, Wang J, et al. Dual visible-light and NHC-catalyzed radical relay trifunctionalization of unactivated alkenes. *Chem Synth* 2024;4:5. DOI
6. Che G, Yang W, Wang C, Li M, Li X, Pan Q. Efficient photocatalytic oxidative coupling of benzylamine over uranyl-organic frameworks. *Inorg Chem* 2022;61:12301-7. DOI PubMed

7. Gao Z, Lai Y, Tao Y, et al. Creating and tailoring ultrathin two-dimensional uranyl-organic framework nanosheets for boosting photocatalytic oxidation reactions. *Appl Catal B Environ* 2021;297:120485. DOI
8. Gholami A, Amirabad TN, Maddahfar M. Investigation of photovoltaic properties of silver-doped $ZnTiO_3$ nanoparticles. *J Mater Sci Mater Electron* 2017;28:15327-32. DOI
9. Amiri R, Rezaei A, Fattahi N, Pirsaheb M, Rodríguez-Chueca J, Moradi M. Carbon quantum dots decorated Ag/$CuFe_2O_4$ for persulfate-assisted visible light photocatalytic degradation of tetracycline: a comparative study. *J Water Process Eng* 2022;47:102742. DOI
10. Liu X, Xu J, Zhang T, et al. Construction of Ag nanocluster-modified Ag_3PO_4 containing silver vacancies via *in-situ* reduction: with enhancing the photocatalytic degradation activity of sulfamethoxazole. *J Colloid Interface Sci* 2023;629:989-1002. DOI PubMed
11. Jin X, Wu Y, Lin Z, et al. Plasmonic Ag nanoparticles decorated copper-phenylacetylide polymer for visible-light-driven photocatalytic reduction of Cr(VI) and degradation of PPCPs: performance, kinetics, and mechanism. *J Hazard Mater* 2022;425:127599. DOI PubMed
12. Chen J, Ren Q, Ding Y, Xiong C, Guo W. Synthesis of bifunctional composites Ag/BiOCl/diatomite: degradation of tetracycline and evaluation of antimicrobial activity. *J Environ Chem Eng* 2021;9:106476. DOI
13. Zhang Y, Liu J, Kang YS, Zhang XL. Silver based photocatalysts in emerging applications. *Nanoscale* 2022;14:11909-22. DOI PubMed
14. Xu Y, Shi X, Hua R, et al. Remarkably catalytic activity in reduction of 4-nitrophenol and methylene blue by Fe_3O_4@COF supported noble metal nanoparticles. *Appl Catal B Environ* 2020;260:118142. DOI
15. Ma C, Shi F, Liu J, et al. Construction of a novel Ag/AgBr/AgI@SiO_2 composite aerogel with controlled pore structure: efficient removal of tetracycline by adsorption/photocatalysis synergism under visible light irradiation. *J Environ Chem Eng* 2023;11:110157. DOI
16. Dutta P, Wang B. Zeolite-supported silver as antimicrobial agents. *Coord Chem Rev* 2019;383:1-29. DOI
17. Ren Z, Chen F, Wen K, Lu J. Enhanced photocatalytic activity for tetracyclines degradation with Ag modified g-C_3N_4 composite under visible light. *J Photoch Photobio A* 2020;389:112217. DOI
18. Zhang Z, Gai H, Li Q, et al. Effect anions on the hydrogenation of nitrobenzene over N-rich Poly(ionic liquid) supported Pd catalyst. *Chem Eng J* 2022;429:132224. DOI
19. Huang X, Lin D, Duan P, et al. Space-confined growth of nanoscale metal-organic frameworks/Pd in hollow mesoporous silica for highly efficient catalytic reduction of 4-nitrophenol. *J Colloid Interface Sci* 2023;629:55-64. DOI PubMed
20. Chen T, Liu Z, Zhang K, et al. Mussel-inspired Ag NPs immobilized on melamine sponge for reduction of 4-nitrophenol, antibacterial applications and its superhydrophobic derivative for oil-water separation. *ACS Appl Mater Interfaces* 2021;13:50539-51. DOI PubMed
21. Zhao X, Wang Y, Zhai Z, et al. Ultrafine Pd on a La metal–organic framework for selective hydrogenation of furfural via a metal–support electronic effect. *ACS Appl Nano Mater* 2023;6:8315-24. DOI
22. Liu L, Su X, Qi M, Gao X, Ren H, Chen L. Facile synthesis of heteroporous covalent organic frameworks with dual linkages: a "three-in-one" strategy. *Chem Synth* 2024;4:10. DOI
23. Xiong XH, Yu ZW, Gong LL, et al. Ammoniating covalent organic framework (COF) for high-performance and selective extraction of toxic and radioactive uranium ions. *Adv Sci* 2019;6:1900547. DOI PubMed PMC
24. Wang Z, Jiang H, Tian Y, Zou X, Zhu G. Porous aromatic frameworks with engineered properties for gas separation membranes. *Trends Chem* 2023;5:446-59. DOI
25. Li J, Cheng Z, Wang Z, et al. Ultramicroporous covalent organic framework nanosheets with functionality pair for membrane C_2H_2/C_2H_4 separation. *Angew Chem Int Ed Engl* 2023;62:e202216675. DOI PubMed
26. Wu J, Liu J, Wen B, et al. Nitrogen-rich covalent triazine frameworks for high-efficient removal of anion dyes and the synergistic adsorption of cationic dyes. *Chemosphere* 2021;272:129622. DOI PubMed
27. Tian Y, Zhu G. Porous aromatic frameworks (PAFs). *Chem Rev* 2020;120:8934-86. DOI PubMed
28. Wu Z, Zhu J, Wen W, Zhang X, Wang S. Spherical covalent organic framework supported Cu/Ag bimetallic nanoparticles with highly catalytic activity for reduction of 4-nitrophenol. *J Solid State Chem* 2022;311:123116. DOI
29. Jing LP, Sun JS, Sun F, Chen P, Zhu G. Porous aromatic framework with mesopores as a platform for a super-efficient heterogeneous Pd-based organometallic catalysis. *Chem Sci* 2018;9:3523-30. DOI PubMed PMC
30. Xu F, Liang B, Liu L, Hu X, Weng B. Pd nanoparticle-decorated covalent organic frameworks for enhanced photocatalytic tetracycline hydrochloride degradation and hydrogen evolution. *Chem Commun* 2023;59:6387-90. DOI PubMed
31. Wang W, Liu C, Zhang M, et al. In situ synthesis of 2D/2D MXene-COF heterostructure anchored with Ag nanoparticles for enhancing Schottky photocatalytic antibacterial efficiency under visible light. *J Colloid Interface Sci* 2022;608:735-48. DOI PubMed
32. Shi W, Lv H, Yuan S, Huang H, Liu Y, Kang Z. Near-infrared light photocatalytic ability for degradation of tetracycline using carbon dots modified Ag/AgBr nanocomposites. *Sep Purif Technol* 2017;174:75-83. DOI
33. Gao R, Choi N, Chang SI, Lee EK, Choo J. Real-time analysis of diaquat dibromide monohydrate in water with a SERS-based integrated microdroplet sensor. *Nanoscale* 2014;6:8781-6. DOI PubMed
34. Shi Z, Chen Z, Zhang Y, et al. COF TzDa/Ag/AgBr Z-scheme heterojunction photocatalyst for efficient visible light driven elimination of antibiotics tetracycline and heavy metal ion Cr(VI). *Sep Purif Technol* 2022;288:120717. DOI
35. Yadav D, Awasthi SK. A Pd confined hierarchically conjugated covalent organic polymer for hydrogenation of nitroaromatics:

catalysis, kinetics, thermodynamics and mechanism. *Green Chem* 2020;22:4295-303. DOI

36. Wang L, Xu H, Qiu Y, et al. Utilization of Ag nanoparticles anchored in covalent organic frameworks for mercury removal from acidic waste water. *J Hazard Mater* 2020;389:121824. DOI PubMed
37. Ma T, Zhao R, Li Z, et al. Efficient gold recovery from E-waste via a chelate-containing porous aromatic framework. *ACS Appl Mater Interfaces* 2020;12:30474-82. DOI PubMed
38. Li H, Luo X, Chen M, et al. Porous organic polymers involving chloro-substituted peryleneimide for photocatalytic water oxidation under visible light irradiation. *Chem Eng J* 2022;443:136463. DOI
39. Li Y, Hu Y, Liu Z, Liu T. Construction of self-activating Z-scheme g-C_3N_4/AgCl heterojunctions for enhanced photocatalytic property. *J Phys Chem Solids* 2023;172:111055. DOI
40. Tang P, Ji B, Sun G. Wearable super-adsorptive fibrous equipment *in situ* grafted with porous organic polymers for carcinogenic fumigant defense and detoxification. *J Mater Chem A* 2020;8:24128-36. DOI
41. Gholami A, Maddahfar M. Synthesis and characterization of barium molybdate nanostructures with the aid of amino acids and investigation of its photocatalytic degradation of methyl orange. *J Mater Sci Mater Electron* 2016;27:6773-8. DOI
42. Wang L, Zhang P, Chen K, et al. Synthetic subnanochannels in porous aromatic frameworks accelerate selective water permeation in membrane desalination. *Sci China Mater* 2022;65:1920-8. DOI
43. Liu Y, Kong J, Yuan J, et al. Enhanced photocatalytic activity over flower-like sphere Ag/Ag_2CO_3/$BiVO_4$ plasmonic heterojunction photocatalyst for tetracycline degradation. *Chem Eng J* 2018;331:242-54. DOI
44. Zhou Z, Shen Z, Song C, Li M, Li H, Zhan S. Boosting the activation of molecular oxygen and the degradation of tetracycline over high loading Ag single atomic catalyst. *Water Res* 2021;201:117314. DOI PubMed
45. Xu J, Zhang B, Jia L, Bi N, Zhao T. Metal-enhanced fluorescence detection and degradation of tetracycline by silver nanoparticle-encapsulated halloysite nano-lumen. *J Hazard Mater* 2020;386:121630. DOI PubMed
46. Deng F, Zhao L, Luo X, Luo S, Dionysiou DD. Highly efficient visible-light photocatalytic performance of Ag/$AgIn_5S_8$ for degradation of tetracycline hydrochloride and treatment of real pharmaceutical industry wastewater. *Chem Eng J* 2018;333:423-33. DOI
47. Guo J, Gan W, Ding C, et al. Black phosphorus quantum dots and Ag nanoparticles co-modified TiO_2 nanorod arrays as powerful photocatalyst for tetracycline hydrochloride degradation: pathways, toxicity assessment, and mechanism insight. *Sep Purif Technol* 2022;297:121454. DOI
48. Guo A, Wang X, Liu H, Li X, Yang L, Yang W. Efficient photocatalytic degradation of water contaminants via Ag decorated porphyrin-based organic framework materials. *Surf Interfaces* 2023;38:102843. DOI
49. Wu J, Fang X, Dong H, Lian L, Ma N, Dai W. Bimetallic silver/bismuth-MOFs derived strategy for Ag/AgCl/BiOCl composite with extraordinary visible light-driven photocatalytic activity towards tetracycline. *J Alloys Compd* 2021;877:160262. DOI
50. Zheng X, Chu Y, Miao B, Fan J. Ag-doped Bi_2WO_6/BiOI heterojunction used as photocatalyst for the enhanced degradation of tetracycline under visible-light and biodegradability improvement. *J Alloys Compd* 2022;893:162382. DOI
51. Han D, Guo B, Li Y, et al. Simultaneous photocatalytic degradation and SERS detection of tetracycline with self-sustainable and recyclable ternary PI/TiO_2/Ag flexible microfibers. *Microsyst Nanoeng* 2024;10:39. DOI PubMed PMC
52. Liu J, Li H, Zhang J, Shen Z. Boosting the photocatalytic activation of molecular oxygen and photodegradation of tetracycline: the role of interfacial synergistic effect of cocatalyst and dopants. *J Colloid Interface Sci* 2022;628:637-48. DOI PubMed
53. Lin D, Duan P, Yang W, et al. Facile fabrication of melamine sponge@covalent organic framework composite for enhanced degradation of tetracycline under visible light. *Chem Eng J* 2022;430:132817. DOI
54. Yu X, Huang J, Zhao J, et al. Efficient visible light photocatalytic antibiotic elimination performance induced by nanostructured Ag/AgCl@Ti^{3+}-TiO_2 mesocrystals. *Chem Eng J* 2021;403:126359. DOI
55. Xiao X, Zhang W, Yu J, Sun Y, Zhang Y, Dong F. Mechanistic understanding of ternary Ag/AgCl@$La(OH)_3$ nanorods as novel visible light plasmonic photocatalysts. *Catal Sci Technol* 2016;6:5003-10. DOI
56. Sun L, Yin S, Shen D, et al. Fabricating acid-sensitive controlled PAA@Ag/AgCl/CN photocatalyst with reversible photocatalytic activity transformation. *J Colloid Interface Sci* 2020;580:753-67. DOI PubMed